Monolithically Integrated Programmable Photonic Microwave Filter with Tunable Inter-Ring Coupling

Robert S. Guzzon, Erik J. Norberg, John S. Parker, Leif A. Johansson, and Larry A. Coldren
ECE Department, University of California, Santa Barbara, CA 93106, USA
guzzon@ece.ucsb.edu

***Abstract*—The design and operation of a coupled-ring programmable photonic microwave filter architecture are described. RF measurements of coupled-ring bandpass filters tunable in bandwidth are presented.**

I. Introduction

As microwave filter applications become more demanding, the use of photonic approaches to improve latency, power consumption, and cost of implementation has gained increasing attention. A photonic filter subsystem within a microwave link promises to provide a low loss, high bandwidth, and highly tunable solution for applications such as reconfigurable microwave channelizers, programmable correlators, or dispersion compensation systems [1-2]. Furthermore, photonic integration offers to lower the cost, reduce the size, and improve the stability of such subsystems over bulk optics. Typically, photonic filters realized in bulk optics are limited to the incoherent regime, where the coherence time of the optical source is much smaller than the filter delay ($\tau_{coh} << T_{delay}$). Such systems inherently have all-positive filter coefficients, resulting in a variety of performance drawbacks [1,2]. The stability improvement of integrated systems is such that optically coherent filtering is achievable, eliminating the need for more complex approaches to attain negative filter coefficients.

Previously, we described the basic building block of a programmable microwave channelizing filter integrated in InP-InGaAsP termed a "unit cell" and demonstrated preliminary results [3,4]. Similar designs have been implemented in other material systems [5-7]. Each unit cell is capable of synthesizing up to 3rd order infinite impulse response (IIR) coupled-pole bandpass filters and first order finite impulse response (FIR) zeros. By cascading unit cells, filters with the extinction ratio and free spectral range (FSR) suitable for microwave channelizing filter applications can be obtained. Here, we review the design and operation of the unit cell and present new RF measurements of 2nd and 3rd order coupled ring filters tunable in bandwidth and frequency.

This work was supported by DARPA through the PhASER project; a portion of the work was done in the UCSB nanofabrication facility, part of the NSF funded NNIN network.

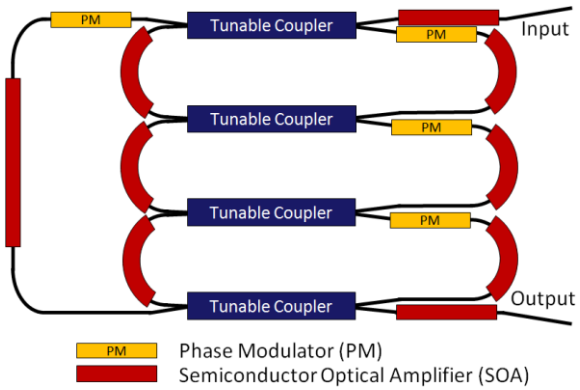

Figure 1. Schematic representation of the unit cell showing SOAs, PMs, MZI Tunable Couplers, and input and output waveguides.

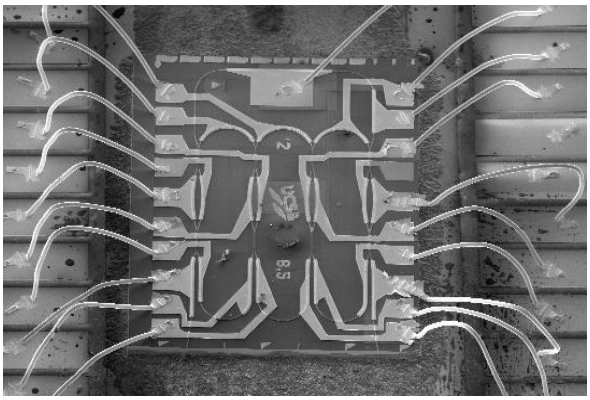

Figure 2. SEM image of a fabricated and wirebonded unit cell. The device measures 1.5 x 2.0mm. Input and output waveguides are at the bottom of the chip.

II. Design and Fabrication

A. Unit Cell Design

Shown in Fig. 1, the unit cell consists of three coupled rings and a bypass waveguide, linked by tunable couplers. An SEM image of a fabricated unit cell is shown in Fig. 2. The rings provide IIR functionality while the bypass waveguide in conjunction with the forward path through the rings supplies the FIR response. The unit cell is capable of synthesizing first order, second order coupled, second order uncoupled, and

third order coupled IIR filters. The tunable couplers consist of a symmetric Mach-Zehnder interferometer (MZI) with phase modulators (PMs) in each 300µm long waveguide. Coupling between waveguides is provided by 2x2 100µm restricted interference multi-mode interference (MMI) couplers [8]. The fabricated tunable couplers show low loss and good tunability with measured cross-coupling extinction down > 20dB from total output power [4]. The ability to attain low coupling values is crucial for synthesis of narrow bandwidth, high extinction ratio filters. Ring loop gain (i.e. pole magnitude) is set by the semiconductor optical amplifiers (SOAs), while the center frequency of each pole is set by the current-injection PMs. Filter bandwidth and pass-band ripple tunability is therefore achieved through adjustment of the coupling values, pole magnitude, and center frequency of each ring. Waveguide paths can be turned off by operating the SOAs in reverse-bias as detectors. This serves 2 purposes: to change the configuration of the unit cell, and to act as on-chip sensors for control feedback.

It is well known that in a coupled-ring system, first order resonances display a splitting caused by higher order poles. For example, in a 2-coupled-ring system, a third pole is created by the "figure 8" path. When the two coupled rings are tuned so that their independent resonances occur at the same wavelength, a splitting will occur (see [9] for a description of the transfer function of such systems). In this way, with the appropriate tuning of SOA gain, a flat-top bandpass filter response can be achieved. Alternatively, if the unit cell is operated in the uncoupled regime, a similar response can be created by tuning the individual pole locations until the desired flat-top filter is synthesized. Each of these configurations is simulated in Fig. 3. The higher order poles created by a coupled system increase roll-off and extinction compared to the uncoupled system.

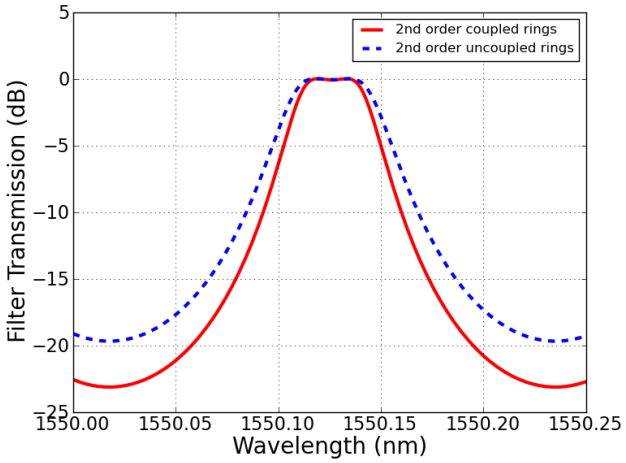

Figure 3. Simulation of 2nd order filters created with coupled and uncoupled rings. Both filters have pole magnitudes of 0.65. Inter-ring coupling of 15% creates the splitting for the coupled ring filter, while a filter displaying similar pass-band ripple with uncoupled rings is synthesized using a phase offset of 0.95 radians. Higher order poles from the coupled ring geometry provide an extra 3.5dB extinction.

The 3mm rings provide ~37ps of delay, resulting in a 27.3 GHz FSR. With reasonable pole magnitudes (0.8-0.9), this ring delay can produce flat-topped filters with bandwidths down to ~ 2GHz. The design can easily be scaled to narrower bandwidths by increasing the ring lengths. The extinction ratio of a filter can be enhanced by cascading multiple unit cells, each producing a copy of the filter, or by cascading IIR bandpass filters with FIR zeros placed in the stop-band. The FSR can be widened by using subsequent unit cells to synthesize FIR zeros, eliminating neighboring filter images [4].

B. Material Structure

The InP/InGaAsP material system provides the phase modulation and optical gain needed for a highly tunable filter architecture. Free-carrier absorption provides phase modulation through current injection, and quantum wells provide gain centered at 1550nm. While gain is crucial to reduce end-to-end loss in large systems, the dynamic range is an important consideration in system design. The system spurious free dynamic range (SFDR) is related to the linearity, and hence the saturation power of the SOAs [10]. To this end, the unit cells were fabricated on a high saturation power offset quantum well (OQW) platform. The quantum wells, which are grown on top of a 1.3Q InGaAsP passive waveguide layer, are selectively wet-etched to create low-loss passive waveguide sections. A blanket InP regrowth acts as the p-cladding. Gain and loss characteristics for this material design have been reported [11]. While offering a high 8.4dBm 1-dB saturation power, the OQW structure has reduced gain compared with a centered quantum well design. The unit cell design, however, requires much less than the 260dB/cm provided by this structure, and further improvements in saturation power can be obtained through the use of lower confinement factor designs [12].

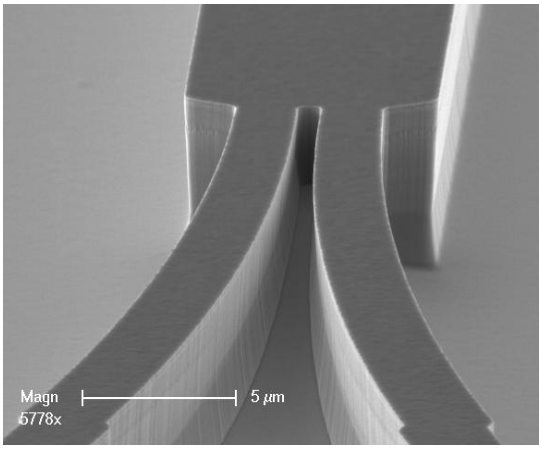

Figure 4. SEM image of the input waveguides to a deep-etched MMI coupler. The restricted interference MMI coupler is 8.5µm wide. Input waveguides are 1.8µm at the MMI coupler, tapering to 2.8µm. All waveguides are etched to a depth of approximately 5.0µm.

C. Fabrication

Fully functional unit cell devices were fabricated. All structures were defined via optical lithography. In order to avoid radiation loss from waveguide bends, high lateral optical confinement waveguides were created with an ICP-RIE "deep etch" process through the waveguide layer. The propagation loss and surface recombination current in these structures have been shown to be comparable to propagation loss and diffusion current in similar width surface ridge

structures. These results and more detail about the fabrication procedure are outlined in [11]. An SEM image of a fully fabricated and wirebonded device is shown in Fig. 2. Fig. 4 shows a close-up SEM image of an MMI coupler.

III. Results

A. Measurement Setup

In order to record filter responses in the RF domain, a single-sideband measurement was conducted using a heterodyne technique with a band-limited noise input. All measurements were conducted with continuous-wave inputs and at room temperature. A schematic representation of the measurement setup is shown in Fig. 5. A white-noise spectrum is generated with an Erbium doped amplified spontaneous emission (ASE) source, and amplified via an Erbium doped fiber amplifier (EDFA). The reflectance spectrum of a fiber grating is utilized to band-limit the input to 0.3nm (37.2GHz), with an out of band rejection of 30dB. The filter response of interest is placed within the band of the input signal, and after propagation through the integrated device the signal is combined with a local oscillator (LO) laser in a 3dB coupler and impinged upon a detector. The wavelength of the laser is chosen such that it falls at the edge of the signal band. In this way, only the lower sideband (in frequency) of the LO is occupied by the band-limited signal. With sufficient suppression, the resultant heterodyned signal measured in an electrical spectrum analyzer (ESA) is effectively single-sideband.

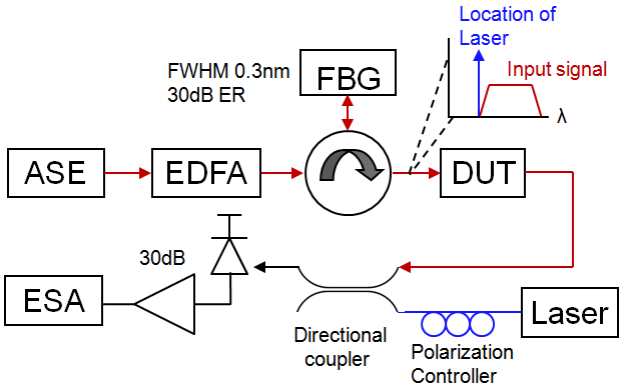

Figure 5. Schematic of the measurement setup.

B. Filter Results

IIR bandpass filters were measured on an ESA with high resolution (10MHz) using the technique outlined above. All data is normalized in frequency and amplitude; however, all filters are tunable across a full FSR – providing the ability to synthesize filters across the entire gain bandwidth and optical telecom band (~1530-1570nm). These filters were measured with a center frequency of about 25GHz. Within the filter pass-band, the signal typically sees on-chip gain of a few dB. Additional gain can be set by the inter-stage SOAs located before and after the unit cell. Maintaining zero to positive net gain would be crucial in a system with many cascaded unit cells where accumulated loss is damaging to the system dynamic range and SNR. Fig. 6 and 7 display 2nd and 3rd order coupled filter results, measured in the RF domain. Bandwidths vary from 3GHz to 7.4GHz and single-stage extinction is as high as 39.5dB. Passband ripple is on the order of 0.5dB. By cascading two stages of the narrowest 3rd order IIR bandpass filter, extinction would be increased to 79dB. If an FIR zero is cascaded with an IIR bandpass filter, the FSR would effectively be doubled to 54.6GHz.

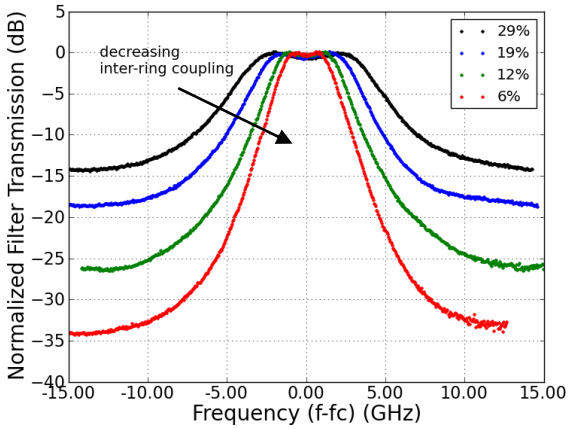

6. Measured 2nd order coupled ring filters for various inter-ring coupling ratios. Lower coupling ratios reduce the pole splitting and result in a filter with lower bandwidth and higher extinction.

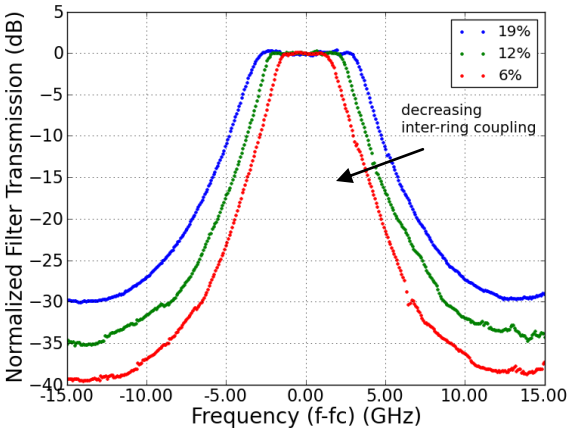

Figure 7. Measured 3rd order coupled ring filters for various inter-ring coupling ratios. For a given inter-ring coupling value, 3rd order filters have wider bandwidth, but show higher extinction and improved rolloff.

IV. Conclusion

RF measurements of programmable microwave photonic filters were presented. 2nd and 3rd order coupled ring filters were synthesized with varying inter-ring coupling to achieve tunable bandwidth. With the ability to place these filters across the full optical telecom band, the presented filter architecture is a viable building block for applications such as tunable microwave channelizing. More elaborate filter shapes, improved FSR, and increased extinction can be attained by cascading independently tunable unit cells.

REFERENCES

[1] J. Campany, B. Ortega, D. Pastor, "A tutorial on Microwave Photonic Filters," *J. of Lightw. Technol.*, vol. 24, no. 1, Jan 2006.

[2] J. Yao, "Microwave Photonics," *J. of Lightw. Technol*., vol. 27, no. 3, Feb. 2009.

[3] E. J. Norberg, R. S. Guzzon, S. C. Nicholes, J. S. Parker and L. A. Coldren, "Programmable Photonic Lattice Filters in InGaAsP-InP," *Photonics Technology Letters*, vol. 22, no.2, pp. 109-111, Jan. 2010.

[4] R. S. Guzzon, E. J. Norberg, J. S. Parker and L. A. Coldren, "Highly Programmable Optical Filters Integrated in InP-InGaAsP with Tunable Inter-ring Coupling," *IPR*, 2010, in press.

[5] H.W. Chen, A. W. Fang, J. Bovington, J. Peters and J. Bowers, "Hybrid silicon tunable filter based on a Mach-Zehnder interferometer and ring resonantor," *Proc. Microwave Photonics*, pp. 1-4, 2009.

[6] P. Toliver *et al*., "A programmable Optical Filter Unit Cell Element for High Resolution RF Signal Processing in Silicon Photonics," Proc. *OFC/NFOEC*, OWJ4, 2010.

[7] S. Ibrahim *et al.*, "Fully Reconfigurable Silicon Photonic Lattice Filters with Four Cascaded Unit Cells," Proc. *OFC/NFOEC*, OWJ4, 2010.

[8] L. Soldano, E. Pennings, "Optical multi-mode intereference devices based on self-imaging: principles and applications," *J. of Lightw. Technol.*, vol. 13, pp. 615-627, 1995.

[9] P. Saeung, P. Yupapin, "Generalized analysis of multiple ring resonator filters: Modeling by using a graphical approach," *Optik*, vol. 119, pp. 465-472, 2008.

[10] P. Berger, J. Bourderionnet, M. Alouini, F. Bretenaker, and D. Dolfi, "Theoretical Study of Spurious-Free Dynamic Range on a Tunable Delay Line based on Slow Light in SOA," *Opt. Exp.*, vol. 17, no. 22, 2009.

[11] E. J. Norberg, R. S. Guzzon, S. C. Nicholes, J. S. Parker and L. A. Coldren, "Programmable photonic filters fabricated with deeply etched waveguides," *Proc. Indium Phosphide & Related Materials*, pp.163-166, 2009.

[12] J. Raring, et al., "Advanced integration schemes for high-functionality/high-performance photonic integrated circuits," *Proc. SPIE*. vol. 6126, 2006.